

Bis(μ -oxo) versus mono(μ -oxo)dicopper cores in a zeolite for converting methane to methanol: in situ XAS and DFT studies

Evalyn Mae C. Alayon, Maarten Nachtegaal, Andras Bodi, Marco Ranocchiari, and Jeroen A. van Bokhoven

Electronic Supporting Information

1. XAS spectra of Cu reference compounds versus those of Cu-MOR, generation of XANES Linear Combination Fit (LCF) references

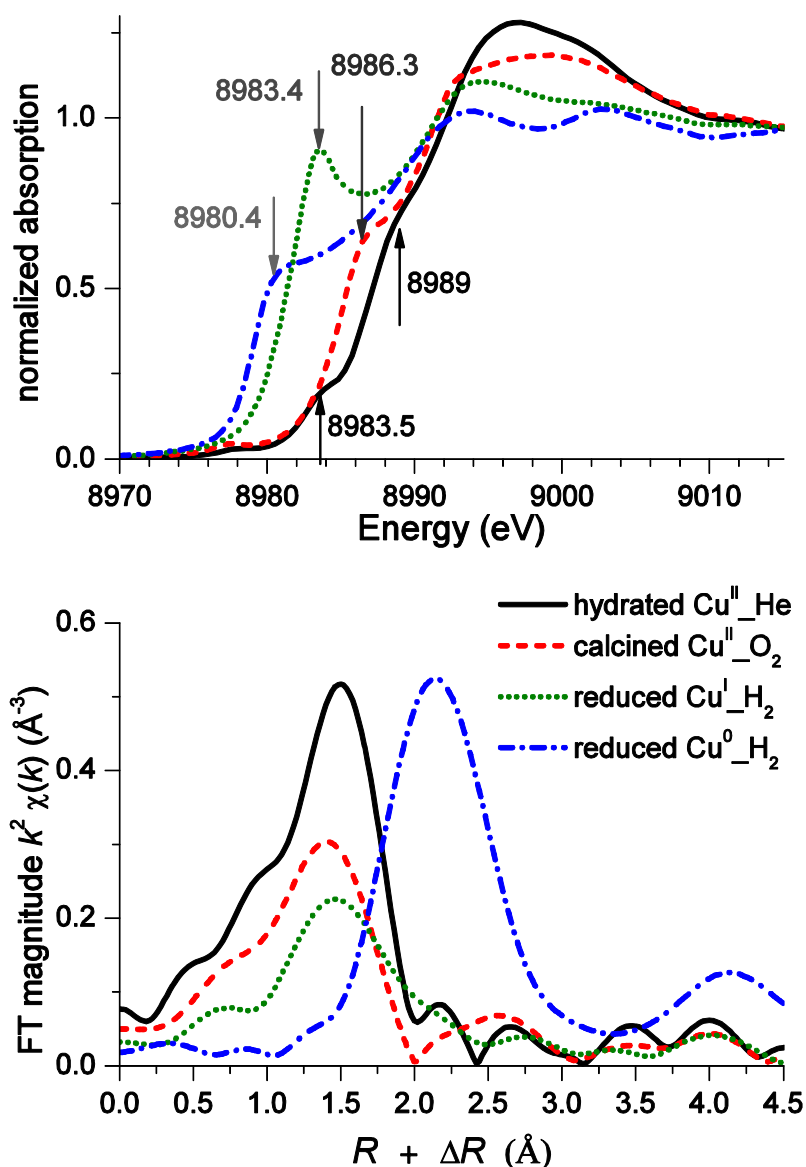


Figure S1-1. XANES and k^2 weighted FT of EXAFS spectra taken of Cu-MOR used as reference spectra for Linear combination fitting. (-) starting hydrated Cu-MOR at RT, (--) calcined in oxygen at 450°C, (•••) reduced in hydrogen to Cu^I at 200°C, and (-•-•-) reduced in hydrogen to Cu⁰ at 450°C.

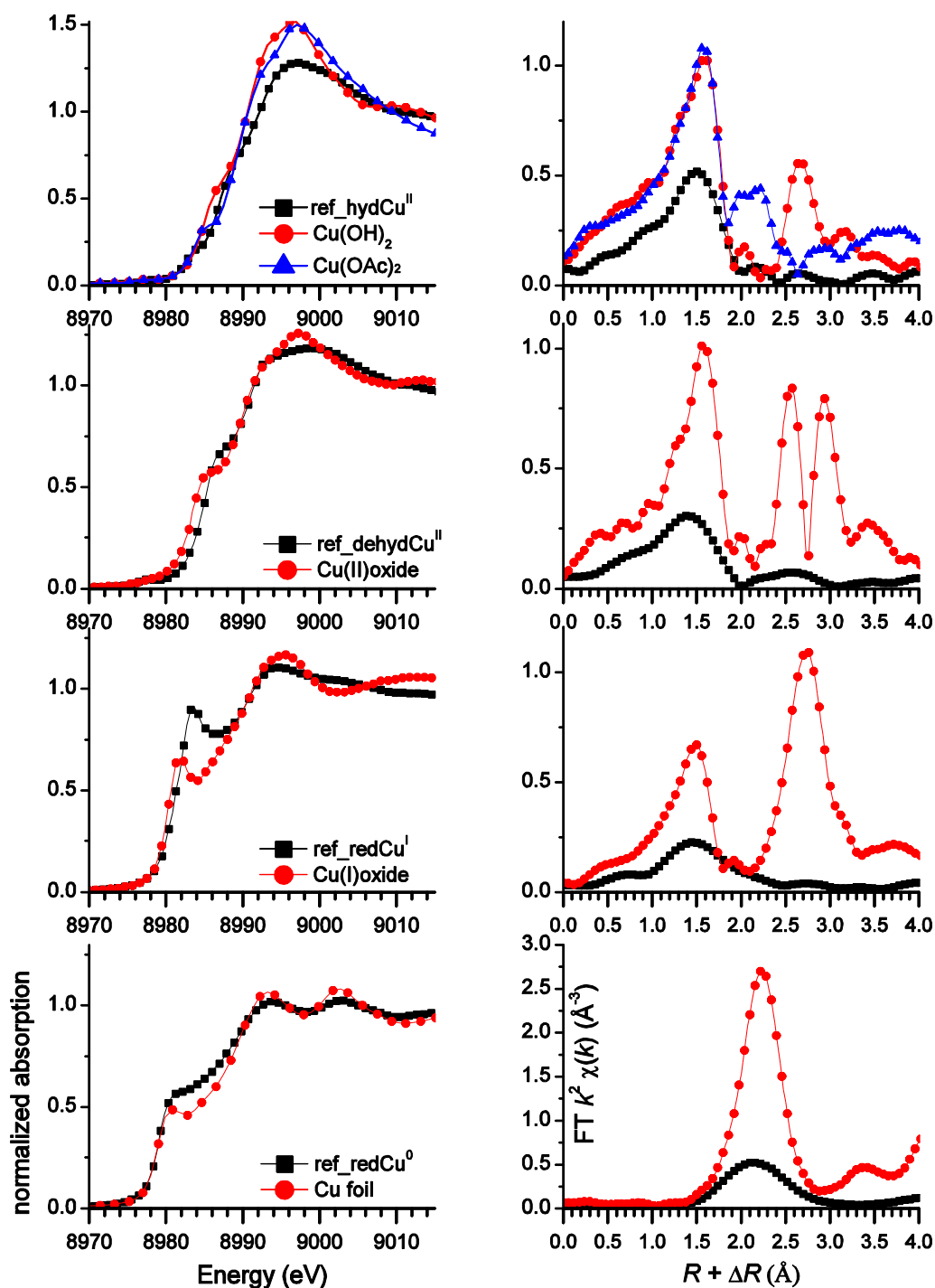


Figure S1-2. Comparison of the XANES and k^2 weighted FT-EXAFS of the reference spectra used for Linear combination fitting to spectra of Cu standard compounds sharing similar XANES features. Differences at maximum absorption (multiple scattering) could be attributed to the lack of long range order in the Cu-MOR samples.

An LCF procedure is normally performed using standard copper compounds for reference spectra, in which the oxidation state and exact structure are known. However, the long range order of these copper structures limit their applicability as references for an LCF for Cu-MOR spectra where the copper species are dispersed and are known to be coordinated to at least two zeolite framework oxygens. Figure S2-2 compares the XANES and FT EXAFS spectra of Cu-MOR with those of standard Cu compounds. The hydrated Cu species of the starting Cu-MOR material was best compared to the structure of copper acetate, which was the synthesis precursor, and copper hydroxide. The XANES spectrum of hydrated Cu-MOR (Figure 4) showed

subtle structure at the rising edge, common to $\text{Cu}(\text{OAc})_2$ and $\text{Cu}(\text{OH})_2$ but its FT EXAFS did not show a defined higher coordination shell. This was directly attributed to the lack of long-range ordering of the Cu sites in Cu-MOR

The XANES spectrum of CuO was similar to that of calcined Cu^{II} -MOR, except for a small shift of the rising edge and an increased intensity at the maximum absorption feature. The FT EXAFS of CuO showed a first coordination shell centered around 1.57 Å corresponding to its first four oxygen neighbors, a second coordination shell centered around 2.55 Å belonging to those of the 2 longer oxygen neighbors, and a third coordination shell centered at 2.94 Å correspond to Cu neighbors at 2.91 – 3.11 Å. The FT EXAFS of Cu^{II} -MOR showed only two coordination shells: one centered around 1.40 Å ($R + \Delta R$) and another centered around 2.55 Å ($R + \Delta R$). The low intensities of these coordination shells and the absence of the distinct Cu-Cu contribution higher than 2.55 Å was a reflection of the minuteness of the Cu clusters in Cu-MOR and the lack of large Cu clusters.

The FT EXAFS spectrum of Cu_2O showed a first coordination shell centered at 1.47 Å, corresponding to the nearest 2 oxygen neighbors. A second coordination shell centered around 2.73 Å was a convolution of Cu (3.02 Å) and O (3.54 Å) backscatterers. The FT EXAFS of Cu^{I} -MOR showed its first coordination shell at a similar distance as that of Cu_2O but with around only 1/3 of the intensity and without the longer backscattering centered at 2.73 Å. This was again a consequence of the absence of long range order of the copper species in Cu-MOR.

The contraction of metal-metal bonds indicated that the copper particles in Cu-MOR are small (few nm). The metal-metal bond length decreases with decreasing particle size especially for particles around 10 Å.

The similarities of the Cu-MOR spectra to the XANES spectra of standard copper compounds in terms of electronic structure but differences in terms of long range order, as seen in the FT EXAFS vouched for their validity as LCF references in the XANES region. Given that size and morphology effects are also reflected in the XANES, care has to be given on the modelling of nanometer-size clusters. The spectrum of metallic Cu foil, for example, is not valid to model Cu clusters, which may have less than 50 atoms.

2. Characterization of starting Cu-MOR

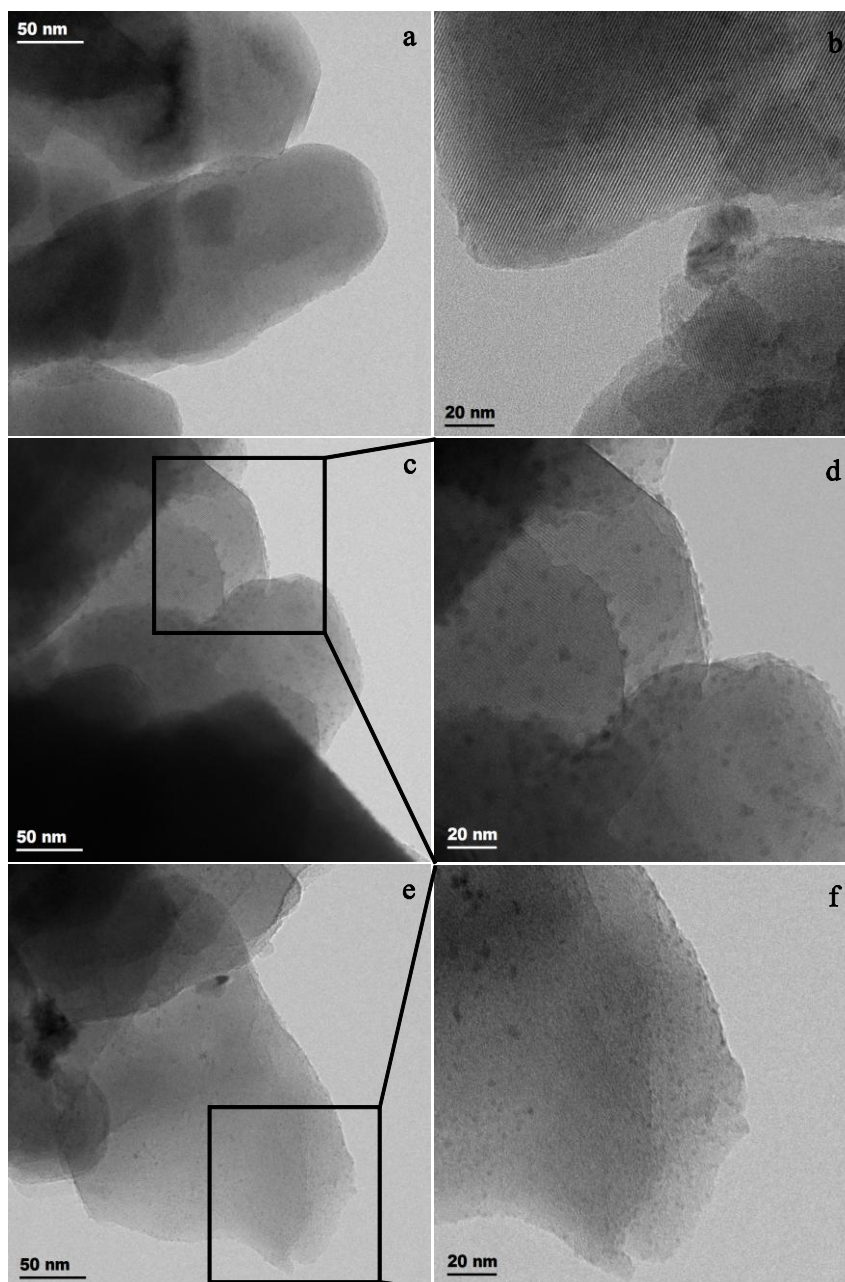


Figure S2-1. TEM micrographs of Cu-MOR after ion exchange and drying (a-d), and after calcination in oxygen at 450 °C (e-f). The size of the Cu particles appears to vary among micrographs; particle sizes are limited to 3 nm and lower.

Figure S2-1 shows TEM images of Cu-MOR after aqueous ion exchange and drying. Figure S2-1b shows Cu-MOR with almost no dark spots that could be attributed to any copper particle while Figure S2-1d shows Cu-MOR having spots/copper particles of about 3-4 nm. This shows that prolonged exposure to the electron beam may cause apparent sintering of copper to particles, in agreement with the findings of Beznis and co-workers (N. V. Beznis, B. M. Weckhuysen and J. H. Bitter, *Catal. Lett.*, 2010, 138, 14-22).

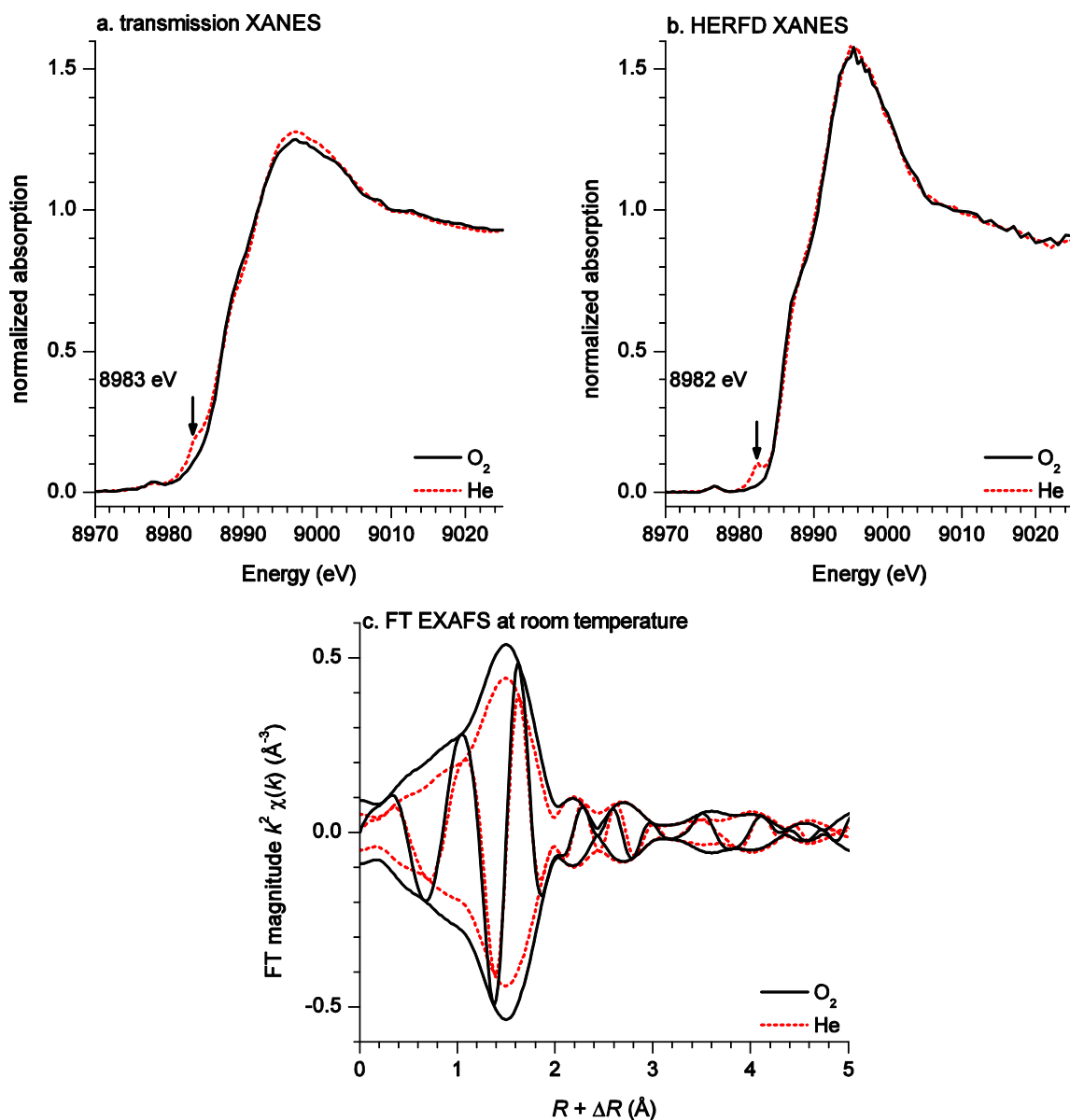


Figure S2-2. XANES spectra of Cu-MOR recorded in (a) transmission and (b) in high resolution in oxygen and helium atmospheres at room temperature after ion exchange and drying, prior to the thermal treatments. The rising edge feature at 8982 – 8983 eV disappeared upon the introduction of oxygen at room temperature, showing the sensitivity of Cu species to the gas environment. (The rising edge feature is similar to that found in the XANES of copper acetate.) The corresponding k^2 weighted FT EXAFS spectra are also shown in (c).

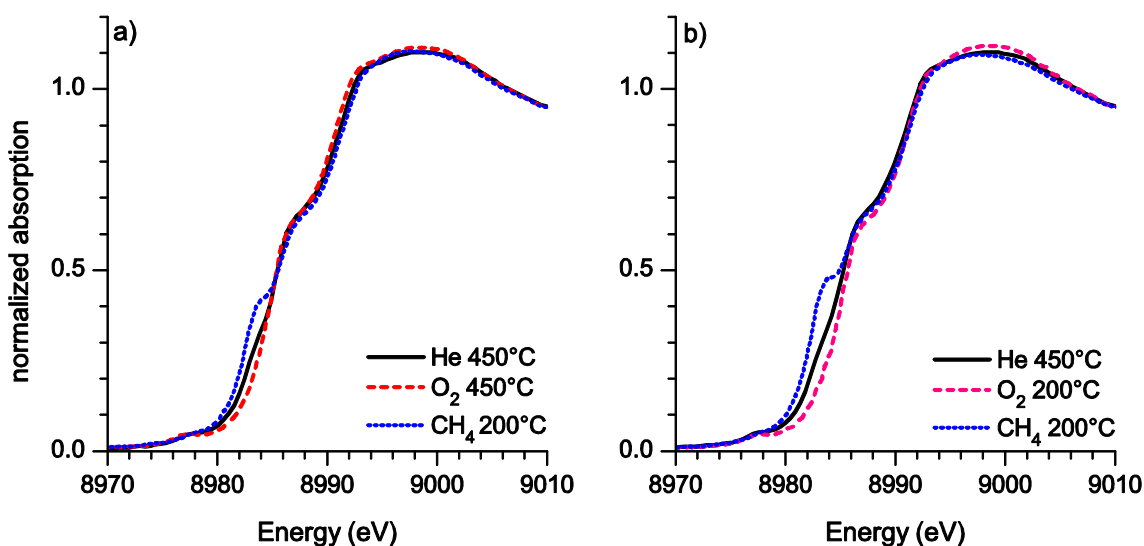


Figure S2-3. XANES spectra of Cu-MOR (a) after thermal treatment helium at 450 °C, reaction with oxygen at 450 °C, and interaction with methane at 200 °C, (b) a subsequent cycle thermal treatment in helium at 450 °C, reaction with oxygen 200 °C, and subsequent reaction with methane at 200 °C. This illustrates the similarity of the redox behavior of the copper sites given sufficient dehydration (and reduction) to cleave molecular oxygen (at both high and low temperatures) and activate methane.

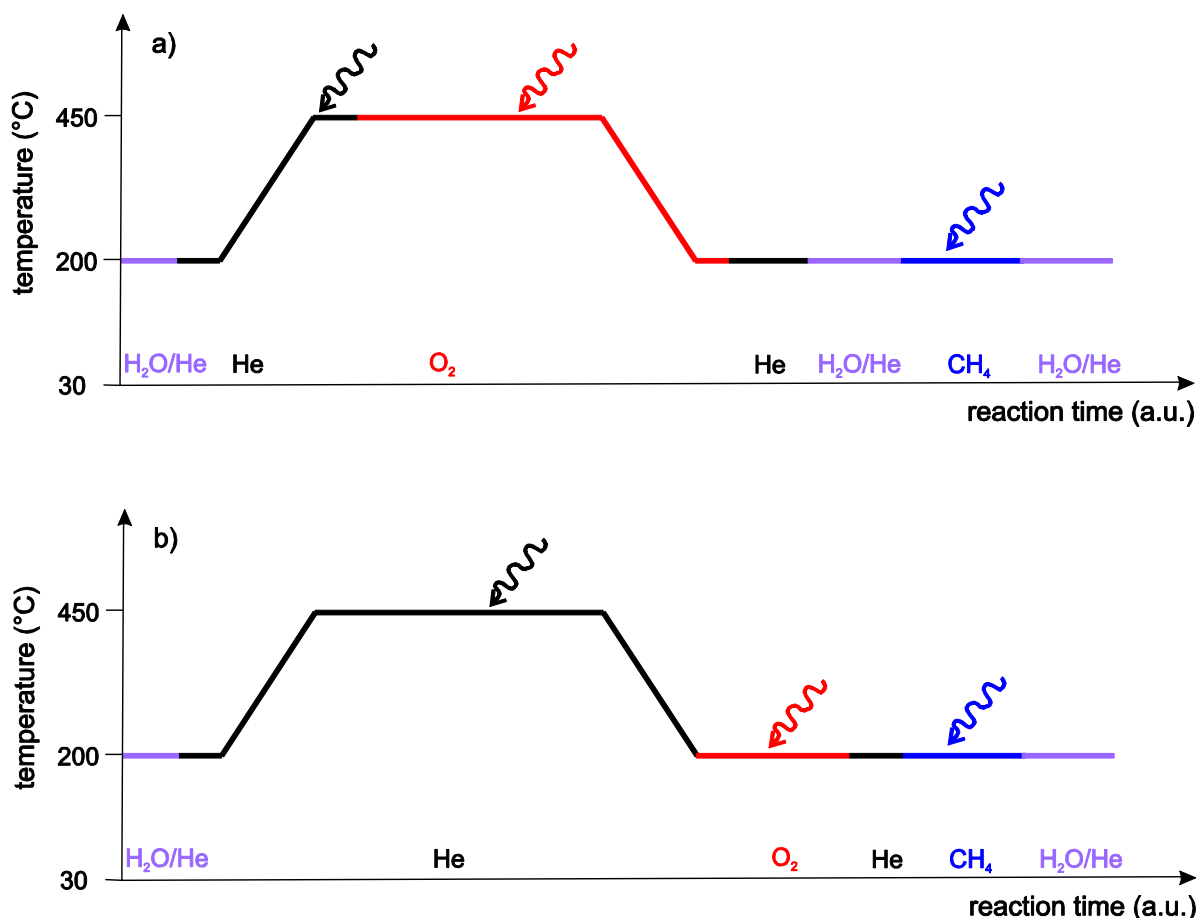


Figure S2-4. Successive treatment schemes for the same sample of Cu-MOR. The curly arrows indicate at which conditions the spectra shown in Figure S2-3 were measured.

Table S2-1. Linear combination fit results of the spectra shown in Figure S2-3.

conditions	LCF components	weight	E_0	R-factor
a) He @ 450 °C	Cu ^{II} -hydrated	0	--	0.000028
	Cu ^{II} -dehydrated	0.85 ± 0.002	0.17	
	Cu ^I	0.15 ± 0.006	0.32	
a) O ₂ @ 450 °C	Cu ^{II} -hydrated	0	--	0.000016
	Cu ^{II} -dehydrated	0.99 ± 0.002	-0.21	
	Cu ^I	0.01 ± 0.006	0.07	
a) CH ₄ @ 200 °C	Cu ^{II} -hydrated	0.18 ± 0.023	0.57	0.000523
	Cu ^{II} -dehydrated	0.51 ± 0.026	0.43	
	Cu ^I	0.31 ± 0.035	0.46	
b) He @ 450 °C	Cu ^{II} -hydrated	0	--	0.000047
	Cu ^{II} -dehydrated	0.84 ± 0.003	-0.03	
	Cu ^I	0.16 ± 0.006	0.10	
b) O ₂ @ 200 °C	Cu ^{II} -hydrated	0.04 ± 0.006	2.34	0.000168
	Cu ^{II} -dehydrated	0.93 ± 0.008	0.04	
	Cu ^I	0.03 ± 0.012	0.23	
b) CH ₄ @ 200 °C	Cu ^{II} -hydrated	0.14 ± 0.017	0.52	0.000294
	Cu ^{II} -dehydrated	0.46 ± 0.019	0.26	
	Cu ^I	0.40 ± 0.026	0.33	

a) spectrum corresponding to graph a) in Figure S2-3

b) spectrum corresponding to graph b) in Figure S2-3

3. EXAFS fit results of the Cu-MOR heating series

Since it is tricky to perform a multiple shell fit, a one-shell fit of Cu–O for the 1st coordination shell (1-O₁) was first performed throughout the data series. In the fitting to the 2nd coordination shell, the contributions of aluminum or silicon backscattering were ruled out, judging from the unfavorable fit results. The assymetrical shape of the 2nd shell, especially at 300 °C and above, prompted the inclusion of two scatterers, 2-O₂ and 3-Cu₁. Finally, the inclusion of the furthest scatterer 4-Cu₂ completed the fit.

Table S3-1. Structural parameters achieved from best fitting of the EXAFS spectra taken of Cu-MOR after synthesis and thermal treatment in oxygen (fit parameters: $3.2 < k < 10.4$, k^2 , $0 < R < 4.5$ Å)

T (°C)	coordination shell	scatterer	N _{fit}	DW (1/Å ²)	R _{fit} (Å)	E ₀ (eV)	goodness of fit
30	1-O ₁	O	3.5 ± 0.02	0.0009 ± 0.00012	1.94 ± 0.001	9.2 ± 0.06	12.0
75	1-O ₁	O	3.3 ± 0.02	0.0014 ± 0.00015	1.92 ± 0.001	10.1 ± 0.08	22.0
	3-Cu ₁	Cu	0.9 ± 0.06	0.0010 ± 0.00084	2.90 ± 0.006	12.0 ± 0.64	
100	1-O ₁	O	3.3 ± 0.03	0.0018 ± 0.00016	1.92 ± 0.001	10.3 ± 0.08	22.6
	3-Cu ₁	Cu	1.0 ± 0.06	0.0020 ± 0.00082	2.90 ± 0.006	12.0 ± 0.60	
150	1-O ₁	O	3.2 ± 0.03	0.0020 ± 0.00017	1.92 ± 0.001	10.4 ± 0.09	22.0
	3-Cu ₁	Cu	1.5 ± 0.10	0.0076 ± 0.00100	2.88 ± 0.007	12.0 ± 0.63	
200	1-O ₁	O	3.2 ± 0.03	0.0031 ± 0.00019	1.90 ± 0.001	10.9 ± 0.10	31.6
	3-Cu ₁	Cu	1.3 ± 0.11	0.0084 ± 0.00130	2.86 ± 0.008	12.0 ± 0.78	
	4-Cu ₂	Cu	2.0 ± 0.22	0.0090 ± 0.00180	4.36 ± 0.010	4.9 ± 0.51	
250	1-O ₁	O	3.0 ± 0.03	0.0028 ± 0.00020	1.90 ± 0.001	11.6 ± 0.11	21.0
	3-Cu ₁	Cu	1.3 ± 0.10	0.0075 ± 0.00130	2.86 ± 0.008	12.0 ± 0.75	
	4-Cu ₂	Cu	2.3 ± 0.22	0.0090 ± 0.00160	4.39 ± 0.009	4.7 ± 0.45	
300	1-O ₁	O	2.7 ± 0.09	0.0029 ± 0.00044	1.90 ± 0.003	12.0 ± 0.40	25.7
	2-O ₂	O	0.2 ± 0.15	0.0000 ± 0.01100	2.42 ± 0.042	0.4 ± 3.38	
	3-Cu ₁	Cu	0.7 ± 0.19	0.0019 ± 0.00300	2.92 ± 0.016	2.3 ± 1.61	
	4-Cu ₂	Cu	1.7 ± 0.24	0.0095 ± 0.00230	4.43 ± 0.014	2.4 ± 0.74	
350	1-O ₁	O	2.8 ± 0.12	0.0038 ± 0.00059	1.89 ± 0.005	12.0 ± 0.54	25.8
	2-O ₂	O	0.2 ± 0.20	0.0000 ± 0.01300	2.38 ± 0.048	3.6 ± 4.46	
	3-Cu ₁	Cu	0.7 ± 0.18	0.0032 ± 0.00290	2.92 ± 0.013	1.7 ± 1.39	
	4-Cu ₂	Cu	2.2 ± 0.27	0.0100 ± 0.00190	4.40 ± 0.012	4.7 ± 0.61	
400	1-O ₁	O	2.7 ± 0.14	0.0038 ± 0.00065	1.90 ± 0.005	12.0 ± 0.63	22.8
	2-O ₂	O	0.2 ± 0.22	0.0000 ± 0.01400	2.38 ± 0.053	4.3 ± 5.23	
	3-Cu ₁	Cu	0.8 ± 0.24	0.0058 ± 0.00360	2.92 ± 0.017	2.1 ± 1.64	
	4-Cu ₂	Cu	2.0 ± 0.27	0.0096 ± 0.00210	4.39 ± 0.013	5.0 ± 0.69	
450	1-O ₁	O	2.6 ± 0.14	0.0044 ± 0.00072	1.90 ± 0.006	12.0 ± 0.70	22.0
	2-O ₂	O	0.2 ± 0.22	0.0000 ± 0.01300	2.37 ± 0.055	3.7 ± 5.48	
	3-Cu ₁	Cu	1.2 ± 0.36	0.0110 ± 0.00400	2.92 ± 0.019	1.6 ± 1.68	
	4-Cu ₂	Cu	2.0 ± 0.26	0.0093 ± 0.00200	4.40 ± 0.013	4.1 ± 0.69	

Table S3-2. Structural parameters achieved from best fitting of the EXAFS spectra taken of Cu-MOR after synthesis and thermal treatment in helium (fit parameters: $3.2 < k < 10.4$, k^2 , $0 < R < 4.5$ Å)

T °C	coordination shell	scatterer	N _{fit}	DW (1/Å ²)	R _{fit} (Å)	E ₀ (eV)	goodness of fit
30	1-O ₁	O	2.5 ± 0.02	-0.0006 ± 0.00015	1.94 ± 0.001	10.3 ± 0.08	11.6
75	1-O ₁	O	2.5 ± 0.02	0.0003 ± 0.00018	1.94 ± 0.001	10.7 ± 0.10	13.1
	2-Cu ₁	Cu	0.5 ± 0.05	0.0000 ± 0.00130	2.95 ± 0.010	12.0 ± 1.06	
100	1-O ₁	O	2.6 ± 0.02	0.0009 ± 0.00018	1.93 ± 0.001	10.4 ± 0.10	17.6
	2-Cu ₁	Cu	0.6 ± 0.05	0.0000 ± 0.00100	2.92 ± 0.008	12.0 ± 0.82	
150	1-O ₁	O	2.4 ± 0.02	0.0015 ± 0.00021	1.92 ± 0.001	10.6 ± 0.11	18.8
	2-Cu ₁	Cu	0.8 ± 0.06	0.0007 ± 0.00086	2.93 ± 0.006	9.2 ± 0.60	
200	1-O ₁	O	2.3 ± 0.02	0.0010 ± 0.00021	1.91 ± 0.001	10.3 ± 0.12	25.7
	2-Cu ₁	Cu	1.0 ± 0.08	0.0041 ± 0.00100	2.90 ± 0.007	10.3 ± 0.69	
	3-Cu ₂	Cu	1.0 ± 0.11	0.0000 ± 0.00140	4.36 ± 0.009	6.4 ± 0.59	
250	1-O ₁	O	2.0 ± 0.03	0.0015 ± 0.00026	1.91 ± 0.001	10.7 ± 0.14	21.0
	2-Cu ₁	Cu	1.2 ± 0.10	0.0072 ± 0.00130	2.88 ± 0.009	12.0 ± 0.81	
	3-Cu ₂	Cu	2.8 ± 0.24	0.0100 ± 0.00140	4.44 ± 0.008	2.6 ± 0.37	
300	1-O ₁	O	1.8 ± 0.02	0.0010 ± 0.00028	1.91 ± 0.002	10.4 ± 0.16	17.3
	2-Cu ₁	Cu	0.9 ± 0.09	0.0067 ± 0.00160	2.86 ± 0.010	12.0 ± 0.99	
	3-Cu ₂	Cu	2.3 ± 0.22	0.0090 ± 0.00160	4.42 ± 0.009	3.3 ± 0.43	
350	1-O ₁	O	1.6 ± 0.02	0.0009 ± 0.00028	1.90 ± 0.002	8.0 ± 0.15	27.2
	2-Cu ₁	Cu	0.9 ± 0.10	0.0092 ± 0.00180	2.99 ± 0.011	-5.0 ± 0.78	
	3-Cu ₂	Cu	2.6 ± 0.24	0.0100 ± 0.00150	4.40 ± 0.008	2.0 ± 0.40	
400	1-O ₁	O	1.5 ± 0.02	0.0013 ± 0.00032	1.90 ± 0.002	9.2 ± 0.17	21.0
	2-Cu ₁	Cu	0.6 ± 0.06	0.0024 ± 0.00150	2.99 ± 0.010	-5.0 ± 0.87	
	3-Cu ₂	Cu	3.0 ± 0.24	0.0100 ± 0.00130	4.36 ± 0.008	4.7 ± 0.39	
450	1-O ₁	O	1.5 ± 0.02	0.0013 ± 0.00032	1.91 ± 0.002	8.9 ± 0.16	19.3
	2-Cu ₁	Cu	0.8 ± 0.11	0.0100 ± 0.00220	3.03 ± 0.012	-5.00 ± 0.86	
	3-Cu ₂	Cu	1.6 ± 0.18	0.0056 ± 0.00160	4.39 ± 0.010	3.6 ± 0.53	

4. Full structures of dicopper species used in Density Functional Calculations

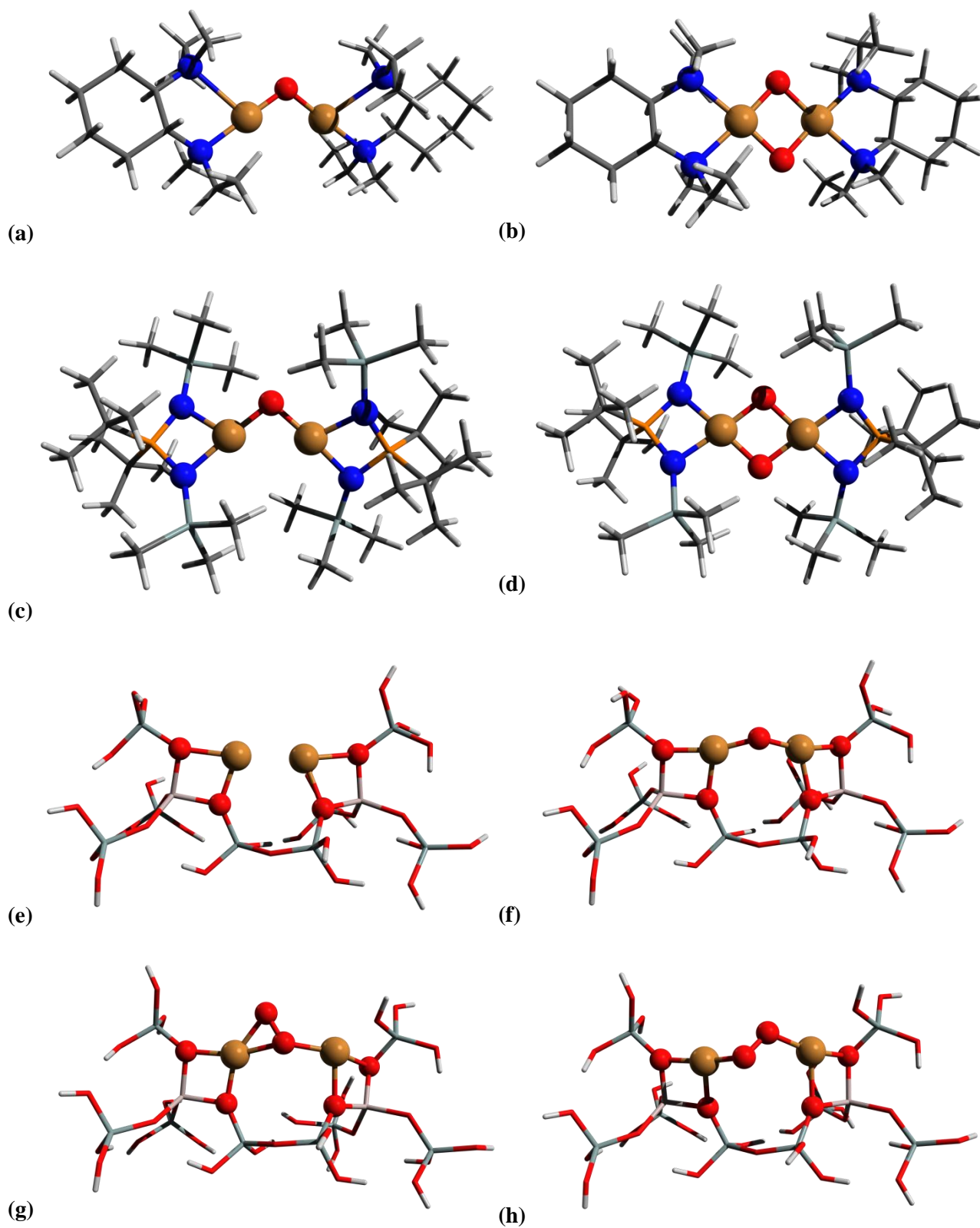
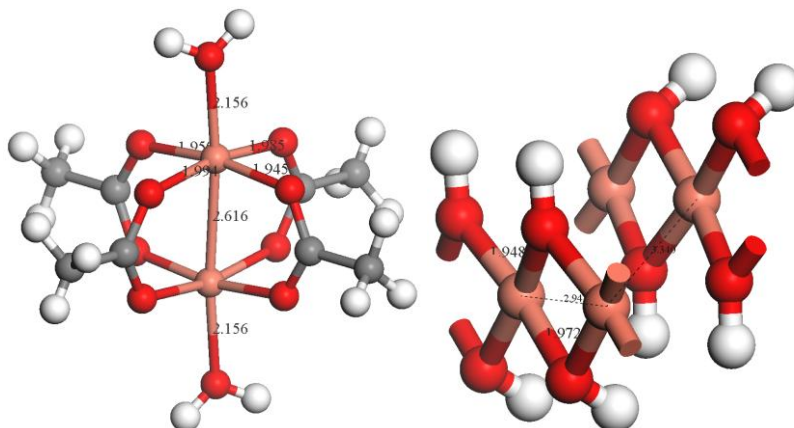


Fig. S4-1. Optimized dicopper complexes and LLM structures: (a,b) [2]-O/O₂, (c,d) [3]-O/O₂, and (e-h) [1-LLM]-O/O/O₂ zeolite model complexes.

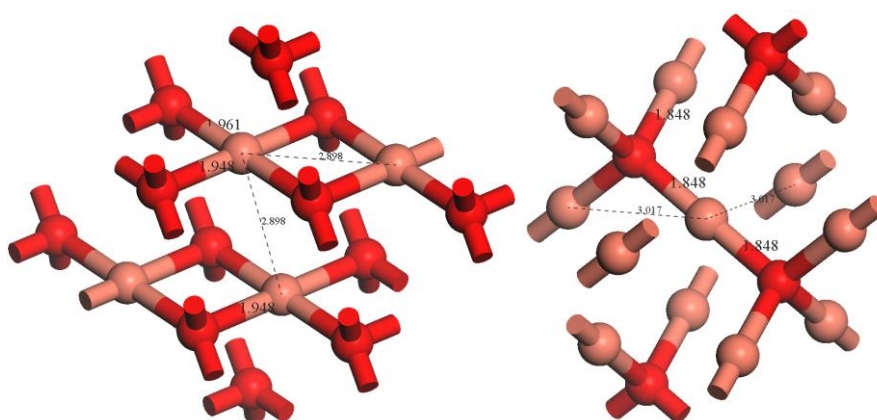
5. Short description of Cu reference compounds



(left) Copper acetate, and (right) copper hydroxide

Copper^{II} acetate. Copper acetate exists as a Cu–Cu dimer and assumes a paddle wheel structure. Each of the copper atoms is coordinated to four planar oxygens (1.97 Å), to a water molecule (2.16 Å) and to a copper atom (2.64 Å). Hydrogen bonds are responsible for the close approach of the two copper atoms.

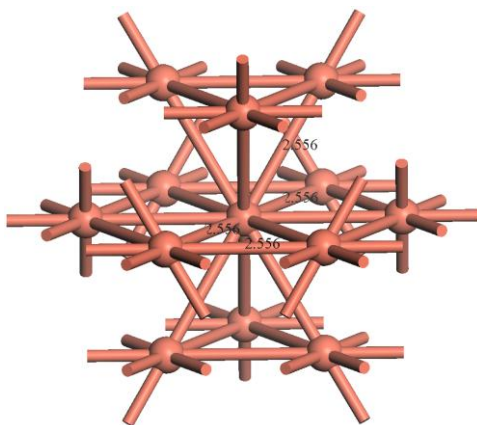
Copper^{II} hydroxide. Cu(OH)₂ takes the form of a distorted octahedron with four planar oxygens and two long apical oxygens (4+1+1). The Cu–O distances are at 1.95 Å and 1.97 Å within the equatorial plane. The Cu–Cu apical distance is 2.36 Å and the other Cu is at 2.92 Å, displaced by 0.13 Å from the equatorial plane. The chains of Cu(OH)₂ octahedra are formed by sharing equatorial edges.



(left) Copper^{II} oxide, and (right) copper^I oxide

Copper^{II} oxide. The nearest oxygen neighbors of copper in cupric oxide form a distorted octahedron (CuO₆ 4+2) with the four nearest oxygens forming a parallelogram, that by sharing sides, make CuO ladders. The four nearest oxygens are at 1.95 – 1.96 Å, the longer oxygens at 2.75 Å, and the nearest copper neighbors at 2.91 Å.

Copper^I oxide. Cuprous oxide is composed of interpenetrated Cu-fcc and O-bcc structures, where copper is linearly coordinated to two nearest oxygen neighbors at 1.85 Å and to 12 copper atoms at 3.02 Å.



Copper⁰. For bulk copper with the first 12 copper neighbors at 2.55 Å, the first shell of copper backscatterers in the FT EXAFS is centered at 2.24 Å. The first shell of copper backscatters for the Cu⁰ species in Cu-MOR was centered at 2.15 Å (fit $N = 7.2$ $R = 2.51$ Å), shorter compared to bulk copper ($N = 12$ $R = 2.55$ Å).